

### **OPEN ACCESS**

EDITED BY Niyazi Bulut, Firat University, Türkiye

REVIEWED BY
Zhenyuan Yin,
Tsinghua University, China
Ziyang Song,
Tsinghua University, China

\*CORRESPONDENCE
Chenglong Yin,

☑ yinchenglong@zjsru.edu.cn

RECEIVED 14 June 2025 ACCEPTED 25 August 2025 PUBLISHED 04 September 2025

### CITATION

Yin C, Huang J, Deng S-y, Ma C and Peng Y (2025) Sodium carbonate and sodium silicate promote the Ca-montmorillonite: the nucleation, stabilization and hydrophilicity mechanisms. Front. Chem. 13:1646971.

### COPYRIGHT

© 2025 Yin, Huang, Deng, Ma and Peng. This is an open-access article distributed under the terms of the Creative Commons Attribution License (CC BY). The use, distribution or reproduction in other forums is permitted, provided the original author(s) and the copyright owner(s) are credited and that the original publication in this journal is cited, in accordance with accepted academic practice. No use, distribution or reproduction is permitted which does not comply with these terms.

# Sodium carbonate and sodium silicate promote the Ca-montmorillonite: the nucleation, stabilization and hydrophilicity mechanisms

Chenglong Yin<sup>1,2\*</sup>, Jin Huang<sup>1</sup>, Shao-yu Deng<sup>1</sup>, Chong Ma<sup>1</sup> and Yong Peng<sup>2</sup>

<sup>1</sup>School of Urban Construction, Zhejiang Shuren University, Hangzhou, China, <sup>2</sup>College of Civil Engineering and Architecture, Zhejiang University, Hangzhou, China

Montmorillonite is widely utilized in catalysis, environmental science, and civil engineering. Previous studies have demonstrated that Na<sub>2</sub>CO<sub>3</sub> and Na<sub>2</sub>SiO<sub>3</sub> enhance the stability of Ca-montmorillonite-rich clayey soils in chemical soil stabilization. However, the microscopic mechanisms underlying their effects on nucleation, stabilization, and hydrophilicity remain unclear. This study investigates these mechanisms using Scanning Electron Microscopy (SEM) and Density Functional Theory (DFT) calculations. SEM results show that Na<sub>2</sub>CO<sub>3</sub> and Na<sub>2</sub>SiO<sub>3</sub> enhance the strength of the stabilized soils by promoting the formation of cementitious and crystalline substances. DFT calculations reveal that SiO<sub>3</sub><sup>2-</sup> and  $CO_3^{2-}$  exhibit the most negative adsorption energies of -6.2 eV and -5.1 eV, respectively, in the exchangeable layers of montmorillonite, significantly higher than those of Na<sup>+</sup> and Ca<sup>2+</sup>. On the montmorillonite surface, SiO<sub>3</sub><sup>2-</sup> and CO<sub>3</sub><sup>2-</sup> display even lower adsorption energies of -8.7 eV and -6.8 eV, respectively. Water molecules preferentially adsorb dissociatively on the montmorillonite surface with an energy of -3.1 eV; however, their adsorption is suppressed following the adsorption of  $Ca^{2+}$ ,  $Na^+$ ,  $CO_3^{2-}$ , and  $SiO_3^{2-}$ , with energies decreasing to between -1.1 eV and -2.5 eV. Differential charge density plots indicate that ion adsorption leads to charge redistribution and the formation of chemical bonds. Specifically, Ca<sup>2+</sup> and Na<sup>+</sup> donate cationic charge, while CO<sub>3</sub><sup>2-</sup> and  $SiO_3^{2-}$  accept electrons. The study further explains why  $Na_2CO_3$  and  $Na_2SiO_3$ , in combination with lime, are more effective than lime alone in soil stabilization. A mechanism model for nucleation, stabilization, and hydrophilicity is proposed to explain the role of  $Na_2CO_3$  and  $Na_2SiO_3$  in promoting Ca-montmorillonite stabilization. This work provides valuable insights into the chemical properties of montmorillonite and the synergistic effects of calcium-based stabilizers combined with  $Na_2CO_3$  and  $Na_2SiO_3$  for soil stabilization.

KEYWORDS

stabilization and hydrophilicity mechanism, Ca-montmorillonite, density functional theory (DFT),  $Na_2CO_3$  and  $Na_2SiO_3$ , soil stabilization, calcium-based stabilizer

### 1 Introduction

Clayey soil is a naturally occurring, multi-scale, and multi-phase mixture formed through geological and biological cycles. Its primary inorganic components are clay minerals—such as montmorillonite, illite, and kaolinite—which are derived from the weathering of rocks during the geological cycle and typically appear as fine, plate-like sheets (Giese and Van Oss, 2002; Mitchell and Soga, 2005). On one hand, these clay minerals possess a large specific surface area and interlayer ion exchange capacity, which make them widely applicable as adsorbents (Zhu et al., 2016), catalysts (Huang et al., 2023), and coagulants (França et al., 2022) in the field of environmental pollution control and remediation. On the other hand, the surfaces of these minerals are generally negatively charged and exhibit high surface free energy, resulting in a strong affinity for water and causing varying degrees of volume expansion upon moisture exposure (Mitchell and Soga, 2005; Petry and Little, 2002). This pronounced sensitivity to moisture fluctuations of clay minerals leads to significant changes in the volume and mechanical strength of clayey soils, thereby posing risks to the stability and safety of buildings and infrastructure constructed on them. Such instability not only compromises structural integrity and public safety but also leads to substantial annual maintenance costs, limiting the broader use of clayey soils—especially those with relatively high water content—in civil engineering applications (Anburuvel, 2023; Pup and pala, 2016).

Soil stabilization is a widely adopted and cost-effective technique for enhancing the engineering properties of fine-grained soils, particularly clayey soils (Anburuvel, 2023; Barman and Dash, 2022; Pup and pala, 2016). This approach typically involves blending various stabilizers into the soils, followed by compaction at an optimal moisture content and a subsequent curing period (Yin et al., 2018; Zada et al., 2023). The fundamental mechanism of soil stabilization relies on utilizing the chemical and/or physicochemical reactions occurred in the stabilizer-soil mixture to modify the surface characteristics and interfacial interactions of soil particles, thus improving the strength, water-resistance and other engineering properties of the soils (Anburuvel, 2023; Barman and Dash, 2022; Mitchell and Soga, 2005; Pup and pala, 2016).

A wide variety of materials have been employed for soil stabilization. Among them, lime and Portland cement—both containing calcium and thus referred to as calcium-based stabilizers—have been among the earliest and most extensively used, due to their widespread availability and well-documented effectiveness (Bell, 1996; Ma et al., 2018; Raja and Thyagaraj, 2020). The stabilization mechanisms of these two calcium-based stabilizers involve a series of reaction processes, including cation exchange, flocculation and agglomeration (particle restructuring), cementitious hydration, hardening, carbonation, and pozzolanic reactions (Anburuvel, 2023; Barman and Dash, 2022; Jiang et al., 2021; Pup and pala, 2016; Wang et al., 2023; Yu et al., 2024).

The introduction of different additives into the calcium-based stabilizer-soil system can alter the reaction processes, resulting in varying stabilization effects. It has been reported that sodium carbonate (Na<sub>2</sub>CO<sub>3</sub>) and sodium silicate (Na<sub>2</sub>SiO<sub>3</sub>) can significantly enhance the strength, water resistance, and other properties of calcium-based stabilized soils (Dengliang and

Aimin, 1988; Murmu et al., 2020; Rivera et al., 2020; Yin et al., 2025). Zhang et al. (Dengliang and Aimin, 1988) conducted a systematic evaluation of the effects of lime-fly ash-based stabilizers with various additives on the compressive strength of stabilizer-soil mixtures. Their results showed that sodium carbonate, sodium silicate, sodium hydroxide, sodium sulfate, and sodium phosphate notably improved the compressive strength of lime-fly ash soils. In our previous study (Yin et al., 2025), we also found that adding only 0.05% sodium carbonate and 0.05% sodium silicate, based on the dry soil weight in solution form, effectively enhanced the 7-day unconfined compressive strength of a calcium-based stabilizer-soil mixture, with the highest strength improvement observed at 34.5%.

The mechanism behind this phenomenon is not yet fully understood. Some researchers have attributed it to the reactions between Ca(OH)<sub>2</sub> and Na<sub>2</sub>CO<sub>3</sub> or Na<sub>2</sub>SiO<sub>3</sub>, as described by the following equations:

$$Ca(OH)_2 + Na_2CO_3 \rightarrow CaCO_3 \downarrow + 2NaOH$$
 (1)

$$Ca(OH)_2 + Na_2SiO_3 \rightarrow CaSiO_3 \downarrow + 2NaOH$$
 (2)

The  $Ca(OH)_2$  is derived from lime and the hydration of Portland cement. The resulting precipitates, calcium carbonate  $(CaCO_3)$  and calcium silicate hydrate (C-S-H), enhance soil stabilization by modifying particle surface characteristics (Chung et al., 2021; Teerawattanasuk and Voottipruex, 2019), filling interparticle voids (Phummiphan et al., 2016; Teerawattanasuk and Voottipruex, 2019), and strengthening interparticle bonding (Abdullah et al., 2021). These processes collectively contribute to the improved macroscopic strength and water resistance of calciumbased stabilized soils. However, the atomic-scale mechanisms that underlie the strength enhancement and hydrophilicity regulation remain poorly understood, particularly in terms of the roles of  $Na_2CO_3$  and  $Na_2SiO_3$  in promoting  $Ca^{2+}$ -clay coordination, modifying the adsorption sites of water molecule, and altering surface charge distribution.

The first-principles method, particularly Density Functional Theory (DFT), is a powerful computational approach for investigating the interaction mechanisms between materials at the atomic and electronic levels. Unlike molecular dynamics (MD) or Monte Carlo (MC) simulations, which primarily rely on classical force fields to model interactions, DFT provides a more fundamental understanding by directly calculating the electronic structure of a system. This allows for deeper insights into the nature of chemical bonds, reaction mechanisms, and material properties. As a result, DFT is particularly well-suited for exploring the interaction mechanisms between clay minerals and various materials. Montmorillonite, with its characteristic 2:1 layered structure and notable properties such as strong water absorption and swelling behavior, is often the preferred clay mineral for DFT-based calculations. Peng et al. (2016) demonstrated that water molecules exhibit distinct adsorption behaviors on different montmorillonite surfaces. On the Na-montmorillonite (001) basal surface, adsorption primarily occurs through electrostatic interactions between water molecules and Na+ cations. In contrast, on the (010) edge surface, hydrogen bonds form between water molecules and surface -OH or -OH2 groups. Miyamoto et al. (Chatterjee et al., 1999) further showed that Na+

TABLE 1 Physical and chemical properties of soil sample.

Natural dry density (g/cm³)	Dried moisture content (%)	Specific gravity	Liquid limit (%)	Plastic limit (%)	Plasticity index	Activity of clay	pH (distilled water)	pH (1M KCl solution)	Carbon content Wt (%)	Sulphur content Wt (%)
1.64	2.94	2.69	37.8	19.3	18.5	2.02	6.55	5.86	1.59~4.25	0~0.77

cations migrate toward the negative charge centers of clay clusters, with each Na<sup>+</sup> cation being coordinated by five interlayer water molecules in montmorillonite. Additionally, studies have explored the adsorption of water molecules by various interlayer cations in montmorillonite (Li et al., 2023), the adsorption of bisphenol by montmorillonite (Guo et al., 2022), and the acid activation process of montmorillonite (Fonseca et al., 2018). While previous studies have focused on water adsorption in montmorillonite, the use of DFT calculations to investigate the molecular nucleation mechanisms of stabilizer-montmorillonite mixtures and their subsequent effects on water adsorption remains limited. Understanding the nucleation and hydrophilicity mechanisms of these mixtures is crucial for gaining a deeper insight into the soil stabilization process. Therefore, this study employs the DFT method to explore these mechanisms.

Based on our preliminary experimental research (Yin et al., 2025), the aim of this study is to investigate the mechanisms by which  $Na_2CO_3$  and  $Na_2SiO_3$  enhance the stability of calcium-based stabilizer-soil mixtures. The morphological changes in the microstructure of the stabilized soils were investigated by SEM scanning. The interactions between  $Ca^{2+}$ ,  $Na^+$ ,  $CO_3^{2-}$  and  $SiO_3^{2-}$  with montmorillonite were examined using DFT calculations. In addition, the surface hydrophilicity before and after stabilization was analyzed, and the adsorption mechanism was explored through differential charge analysis. This work offers a theoretical perspective on the synergistic mechanisms of calcium-based stabilizers in combination with  $Na_2CO_3$  and  $Na_2SiO_3$  in soil stabilization.

### 2 Materials and computation details

### 2.1 Experimental materials

The experimental soil, a type of lean clay predominantly consisting of montmorillonite and other minerals, has its physical and chemical properties detailed in Table 1. For this study, the calcium-based stabilizer, denoted as B2, is a composite mixture of Portland cement (PC), lime (L), and fly ash (FA) with a mass ratio of 4:2:1(PC:L:FA), and the chemical compositions of these three components are illustrated in Table 2. The sodium carbonate (Na<sub>2</sub>CO<sub>3</sub>) and sodium silicate (Na<sub>2</sub>SiO<sub>3</sub> · 9H<sub>2</sub>O) used in the experiments are all analytical pure chemical reagents produced by Shanghai Hushi Laboratory Equipment Co., Ltd (Shanghai, China).

### 2.2 Experimental methods

The experimental procedures primarily consisted of compaction testing, specimen preparation and curing, and unconfined

compression testing, conducted in accordance with the Chinese Standard JTG 3441-2024. Initially, the B2 stabilizer and dried soil were thoroughly mixed in a mass ratio of 4:2:1:100 (PC:L:FA:dry soil), yielding a base mixture. Then the maximum dry density and optimum moisture content of the base mixture were tested to be 1.79 g/cm3 and 15%, respectively, by the modified Proctor compaction test. Subsequently, 0.05% sodium carbonate and 0.05% sodium silicate (calculated relative to the dry soil weight and added in an aqueous solution manner) were then incorporated into part of the base mixture to form a testing mixture. The mixtures with and without the two sodium salts were then statically compacted into cylindrical specimens, each measuring 50 mm in height and 50 mm in diameter, at their optimum moisture content using a 30 kN hydraulic pressing machine. Then, the compacted specimens were transferred to a curing room maintained at a temperature of 20 °C  $\pm$  1 °C and a relative humidity of 95%  $\pm$  5%. After a 7-day curing period, unconfined compression tests were conducted using a 30 kN hydraulic pressing machine at a displacement rate of 1 mm/min.

### 2.3 Experimental characterization

After the compression tests, samples extracted from the tested specimens were subjected to SEM scanning. An FEI Quanta 650 FEG Environmental SEM (ESEM) was employed for the scanning process, operating within an acceleration voltage range of 200V to 30 kV and with a maximum beam current of 200 nA.

### 2.4 DFT computational method

CP2K (Kühne et al., 2020) was employed to carry out the theoretical calculations in the framework of density functional theory (DFT). CP2K employed two representations of the electron density: localized Gaussian and plane wave basis sets. For the Gaussian-based (localized) expansion of the Kohn-Sham orbitals, we used a library of contracted molecularly optimized valence double-zeta plus polarization basis sets (VandeVondele and Hutter, 2007), and the complementary plane wave basis set had a cutoff of 400 Rydberg for the electron density. The generalized gradient corrected approximation of Perdew, Burke and Ernzerhof (PBE) (Blöchl, 1994) was adopted to relax the geometric structures. The energy and force convergence criteria of the self-consistent iteration were set to 10-5 eV and 0.03 eV Å-1. The ions are calculated in a 15 Å  $\times$  15 Å  $\times$  15 Å cell. Since montmorillonite has layered structure, no additional vacuum layer was set, which is consistent with previously reported montmorillonite calculations (Li

Materials	Chemical compositions (Mass fraction, %)									
	SiO <sub>2</sub>	Al <sub>2</sub> O <sub>3</sub>	Fe <sub>2</sub> O <sub>3</sub>	CaO	Na <sub>2</sub> O	K <sub>2</sub> O	MgO	TiO <sub>2</sub>	SO <sub>3</sub>	
PC	18.04	8.79	4.96	54.14	0.12	0.32	3.56	-	1.77	
L	-	-	-	86.26	-	-	0.68	-	-	
FA	11.61	21.73	1.75	40.28	0.95	1.36	0.49	1.66	0.61	

TABLE 2 Chemical composition of the calcium-based stabilizers.

et al., 2023; Peng et al., 2016). During calculation, all atoms remain relaxed.

The adsorption energies were used to assess the adsorption capacity of the montmorillonite models for molecules and ions. The adsorption energy is defined by Formula 3, where  $\Delta E$  represents the adsorption energy, while E (surf), E (ion), and E (ion/surf) denote the total energies of the surface, the free ion, and the surface with the ion, respectively. The more negative the adsorption energy in value, the greater the exothermic heat released, and the more stable the system becomes.

$$\Delta E = E(ion/surf) - E(surf) - E(ion)$$
 (3)

### 2.5 Montmorillonite surface model

Montmorillonite (PDF#13-0135), with the chemical formula CaAl<sub>4</sub>Si<sub>8</sub>O<sub>24</sub>, belongs to the hexagonal crystal system. Figure 1 displays the top and side views of the montmorillonite model. The unit cell parameters are as follows: a=5.169~Å,~b=5.169~Å, c=15.02~Å, with angles  $\alpha=90.0^\circ,~\beta=90.0^\circ,$  and  $\gamma=90.0^\circ.$  In its structure, Ca²+ cations act as exchangeable ions located between the layers, while Al³+ cations reside in the bulk phase. The Si⁴+ cations are tetrahedrally coordinated within the SiO4 units, and the O²-anions are 2-coordinated in the OSi2 environment and 3-coordinated in the OSi42 environment.

### 3 Results and discussion

# 3.1 The strength and microscopic morphological characteristics of the mixtures

The 7-day unconfined compressive strength of the base mixture was determined to be 1.182 MPa. After introducing 0.05% sodium carbonate and 0.05% sodium silicate, the 7-day unconfined compressive strength of the testing mixture escalated to 1.620 MPa, signifying a 34.5% enhancement in strength (Yin et al., 2025).

Figure 2 shows the SEM images of soil samples before and after the addition of Na<sub>2</sub>CO<sub>3</sub> and Na<sub>2</sub>SiO<sub>3</sub>. In the SEM images of the B2 stabilizer-soil mixture, prominent pores can be observed, along with only a small amount of fibrous or reticular cementitious substances and acicular crystals on the particle surfaces (Cao et al., 2022; Wu et al., 2018). After adding Na<sub>2</sub>CO<sub>3</sub> and Na<sub>2</sub>SiO<sub>3</sub>,

the pores are filled with fibrous or reticular cementitious substances and acicular crystals, and similar deposits are observed coating the particle surfaces. This suggests that the addition of Na<sub>2</sub>CO<sub>3</sub> and Na<sub>2</sub>SiO<sub>3</sub> promotes the formation of cementitious and crystalline substances which are deduced to be C-S-H and calcium carbonate according to chemical reaction Equations 1, 2. These newly formed substances effectively modify the surface characteristics of the soil particles, fill interparticle voids, and enhance interparticle bonding. As a result, the strength of the stabilizer-soil mixtures increase from 1.182 MPa to 1.620 MPa, which aligns well with findings reported in previous studies (Abdullah et al., 2021; Chung et al., 2021; Dengliang and Aimin, 1988; Murmu et al., 2020; Phummiphan et al., 2016; Rivera et al., 2020; Teerawattanasuk and Voottipruex, 2019; Yin et al., 2025).

However, the existing techniques are difficult to characterize the microscopic processes and mechanisms of nucleation and crystallization of  $Na_2CO_3$  and  $Na_2SiO_3$  in the pores and on the surface of montmorillonite. Therefore, subsequently, the DFT method was adopted to study their nucleation and crystallization mechanisms as well as physicochemical properties.

# 3.2 Structures and adsorption energies of $Ca^{2+}$ , $Na^+$ , $CO_3^{2-}$ and $SiO_3^{2-}$

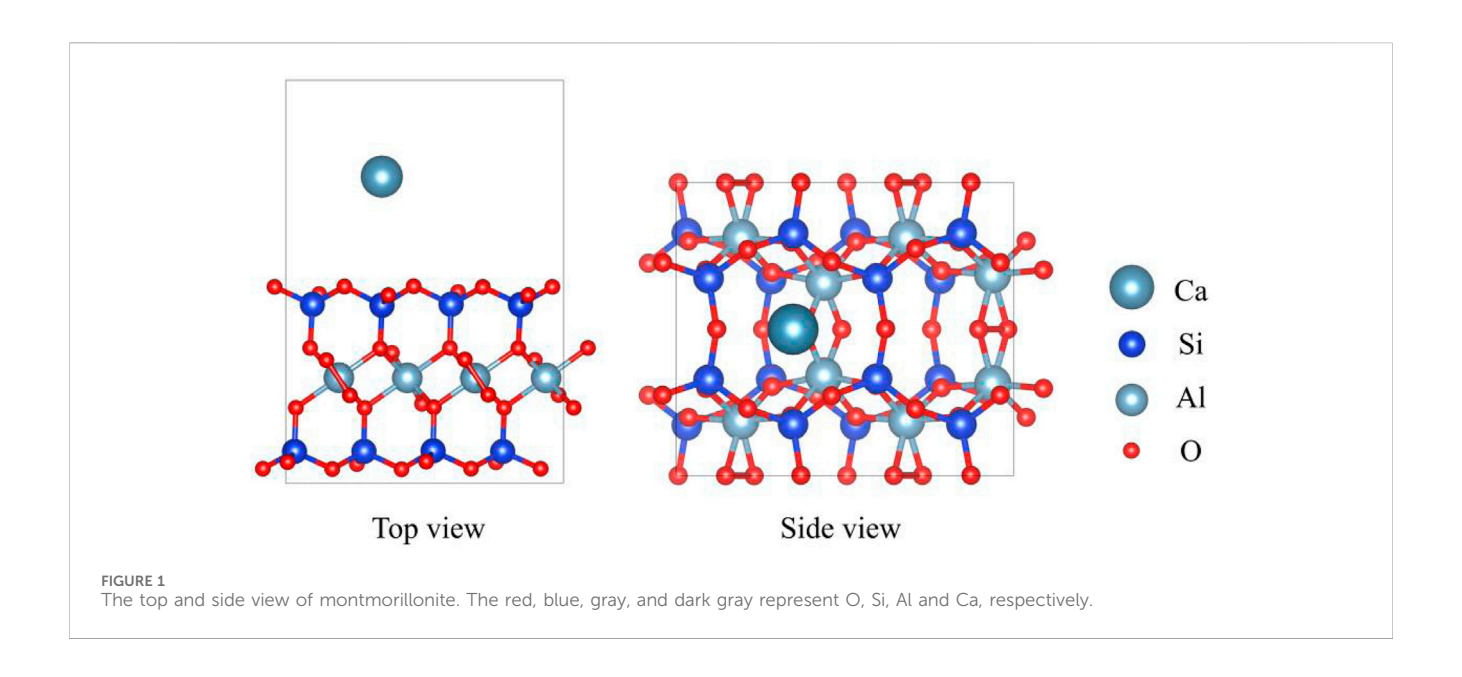
Montmorillonite contains both exchangeable layers and surfaces. Accordingly, the adsorption behaviors of  $Ca^{2+}$ ,  $Na^+$ ,  $CO_3^{2-}$ , and  $SiO_3^{2-}$  in these two distinct scenarios were investigated.

### 3.2.1 On exchangeable layer

Figures 3, 4 show the structures and adsorption energies for the adsorption of  $\text{Ca}^{2+}$ ,  $\text{Na}^+$ ,  $\text{CO}_3^{2-}$ , and  $\text{SiO}_3^{2-}$  on the exchangeable layer of montmorillonite. For  $\text{Ca}^{2+}$  adsorption on the exchangeable layer, the adsorption energy is -1.9 eV. The distance between the two  $\text{Ca}^{2+}$  atom is 518 pm. When  $\text{Na}^+$  adsorbs on the exchangeable layer, its adsorption energy is -2.3 eV, which is slightly higher than that of  $\text{Ca}^{2+}$  on exchangeable layer. The distance between the  $\text{Ca}^{2+}$  and  $\text{Na}^+$  is 428 pm.

For  ${\rm CO_3}^{2^-}$  adsorption on the exchangeable layer,  ${\rm CO_3}^{2^-}$  coordinates with  ${\rm Ca}^{2^+}$  through O. The Ca-O bond length is 193 pm, and the adsorption energy is -5.1 eV. For  ${\rm SiO_3}^{2^-}$  adsorption on the exchangeable layer,  ${\rm SiO_3}^{2^-}$  coordinates with  ${\rm Ca}^{2^+}$  through one O atom. The Ca-O bond length is 191 pm, and the adsorption energy is -6.2 eV.

Thus,  $SiO_3^{2-}$  has the highest adsorption energies, indicating a stronger interaction with the montmorillonite exchangeable layer compared to  $CO_3^{2-}$ ,  $Ca^{2+}$  and  $Na^+$ . The adsorption energy order is



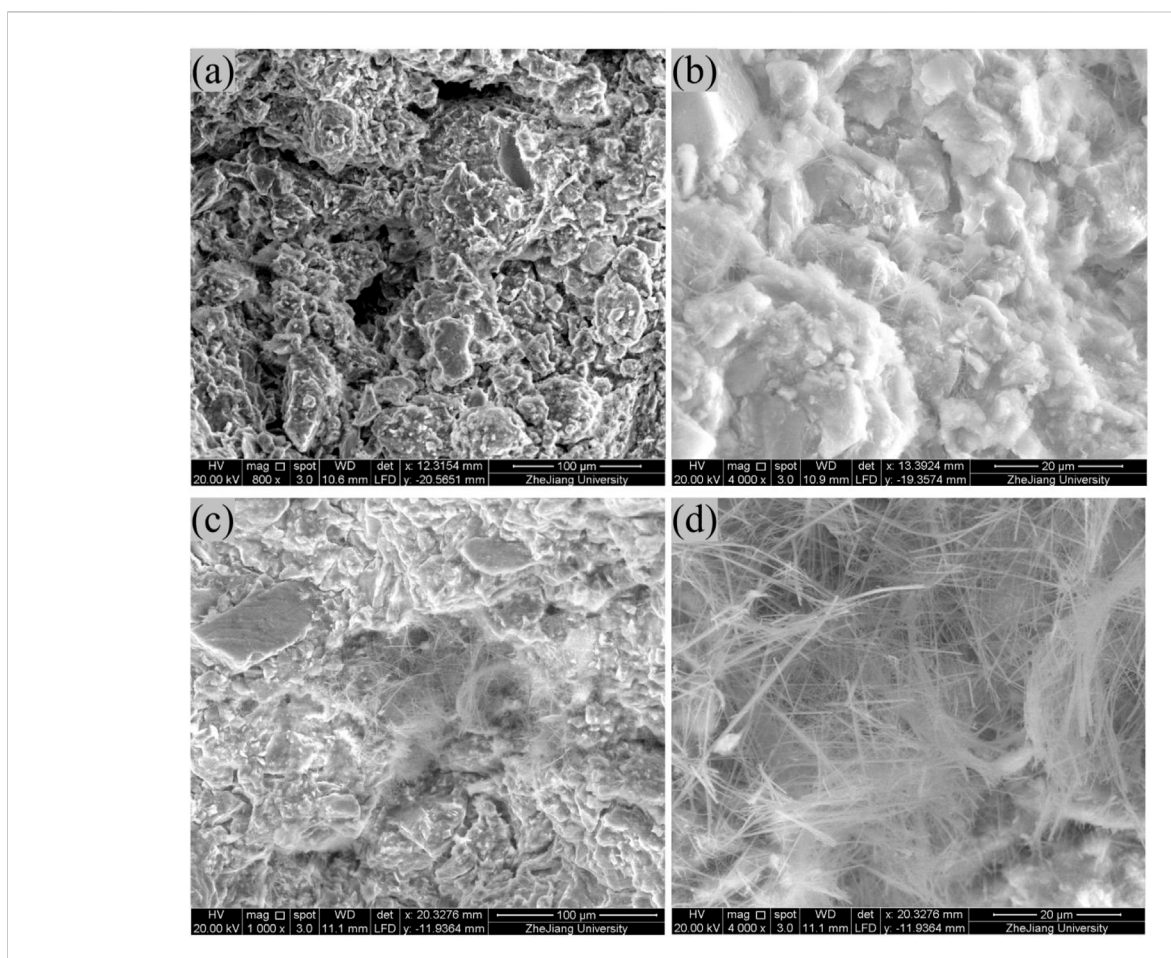
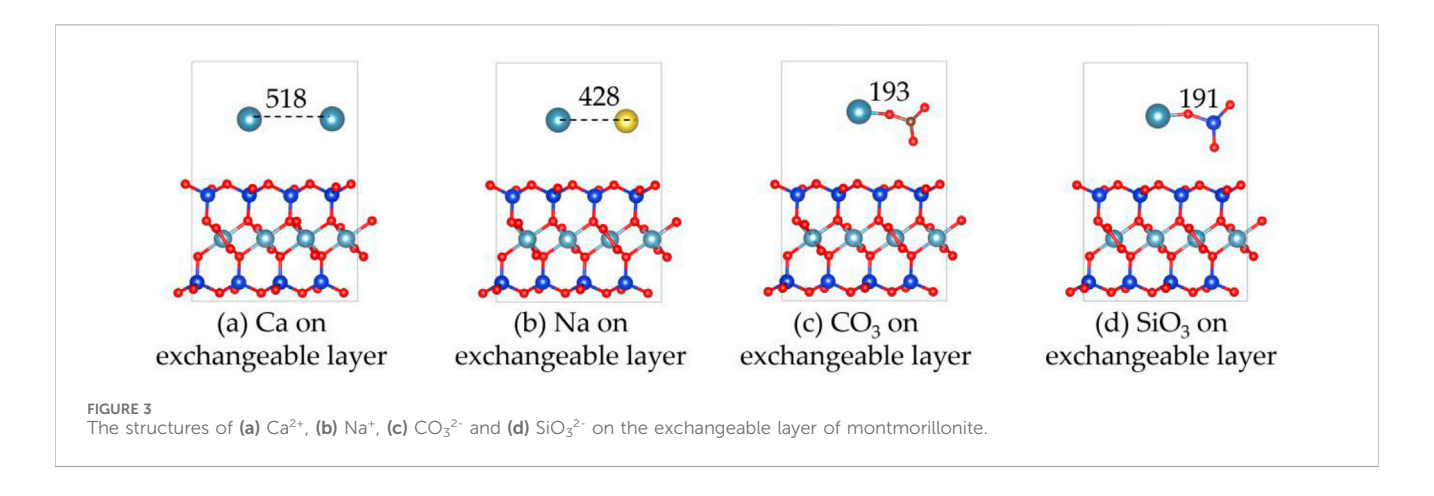
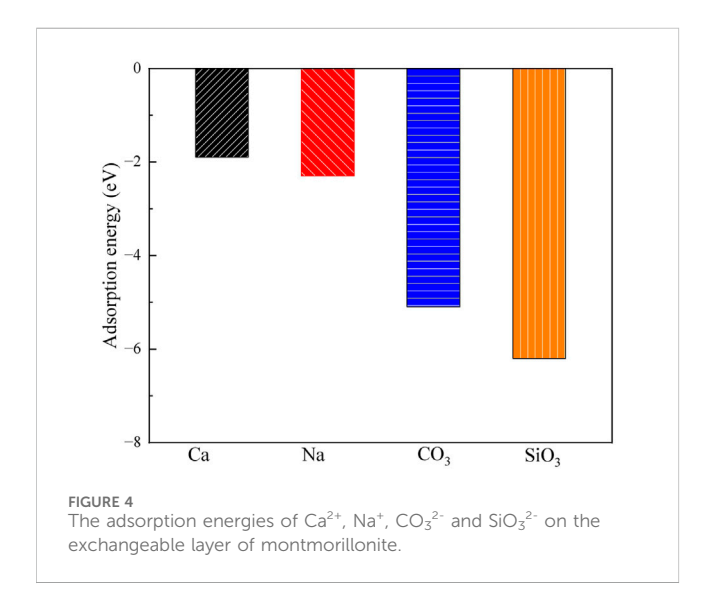


FIGURE 2 SEM images of soil samples (a,b) are the B2 stabilizer-soil mixture without  $Na_2CO_3$  and  $Na_2SiO_3$ ; (c,d) are the B2 stabilizer-soil mixture with the addition of  $Na_2CO_3$  and  $Na_2SiO_3$ .





 $SiO_3^{2-} > CO_3^{2-} >> Na^+ > Ca^{2+}$ . This implies that  $CO_3^{2-}$  and  $SiO_3^{2-}$  are more likely to be stably adsorbed on the layer than that of  $Ca^{2+}$  and  $Na^+$ .

### 3.2.2 On surface

Figures 5, 6 show the structures and adsorption energies for the adsorption of  $Ca^{2+}$ ,  $Na^+$ ,  $CO_3^{2-}$ , and  $SiO_3^{2-}$  on the surface of montmorillonite. For the adsorption of  $Ca^{2+}$  on the surface of montmorillonite, the adsorption energy is - 4.7 eV  $Ca^{2+}$  adsorbs on the surface of montmorillonite by bonding with two O atoms. The bond lengths are 283 pm and 220 pm respectively. This indicates that for  $Ca^{2+}$ , surface adsorption results in a higher adsorption energy and greater stability compared to layer adsorption. In contrast, during layer adsorption, its adsorption energy was only -1.9 eV. The higher adsorption energy during surface adsorption implies a stronger interaction between  $Ca^{2+}$  and the montmorillonite surface, thus making the adsorbed state more stable.

When  $Na^+$  adsorbs on the surface, its adsorption energy is -5.1 eV. The distances between two surface O atoms are 258 pm and 289 pm. The higher adsorption energy compared to  $Ca^{2+}$  suggests that  $Na^+$  has a stronger interaction with the surface.

For the adsorption of  $CO_3^{2-}$  on the surface, the adsorption energy is -6.8 eV  $CO_3^{2-}$  forms bonds with  $Ca^{2+}$  through two O atoms, with Ca-O bond lengths of 215 pm and 209 pm. Additionally,  $CO_3^{2-}$  bonds with a surface Si atom via one O atom, with the O-Si bond length of 201 pm. For the adsorption of  $SiO_3^{2-}$  on the surface, the adsorption energy reaches -8.7 eV, the highest among the four substances.  $SiO_3^{2-}$  forms bonds with  $Ca^{2+}$  through two O atoms, with Ca-O bond lengths of 219 pm and 216 pm, and also bonds with a surface Si atom through one O atom, with O-Si bond length of 185 pm.

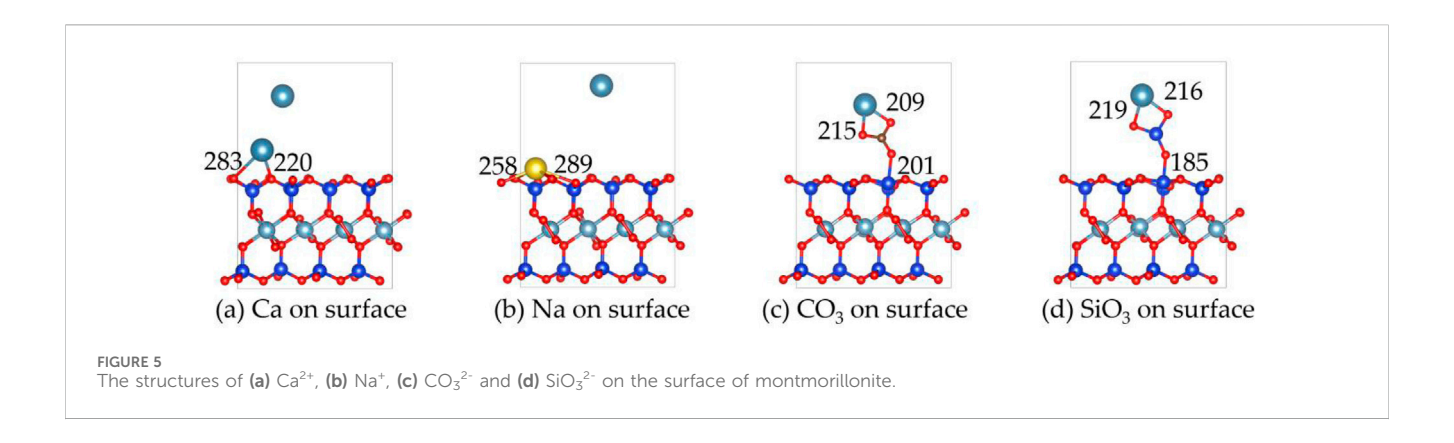
Overall, the order of adsorption energies is  $SiO_3^{2-} > CO_3^{2-} > Na^+ > Ca^{2+}$ . This implies that  $SiO_3^{2-}$  is most likely to be stably adsorbed on the surface, followed by  $Na^+$  and  $SiO_3^{2-}$ , while  $SiO_3^{2-}$  has relatively weaker adsorption stability.

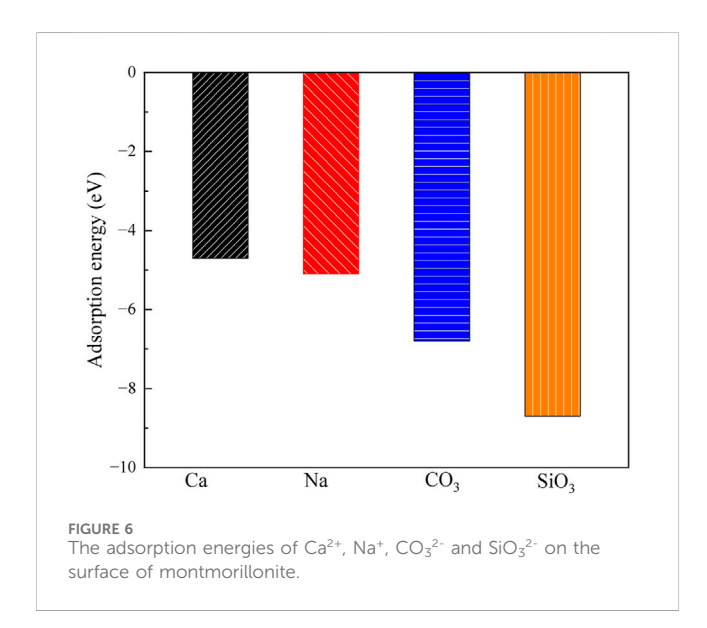
The above study investigated the adsorption behavior of  $Ca^{2+}$ ,  $Na^+$ ,  $CO_3^{2-}$ , and  $SiO_3^{2-}$ . Both  $SiO_3^{2-}$  and  $CO_3^{2-}$  exhibite the most negative adsorption energies on the exchange layer and surface. This proves that  $Na^+$ ,  $CO_3^{2-}$  and  $SiO_3^{2-}$  all contribute to the solidification of  $Ca^{2+}$  and the stability of montmorillonite.

### 3.3 Hydrophilicity of montmorillonite

### 3.3.1 Clean montmorillonite

Figures 7, 8 show the structures and adsorption energies for the adsorption of H<sub>2</sub>O and OH on the montmorillonite. For the H<sub>2</sub>O physical adsorption configuration, the adsorption energy is only -0.1 eV. The H<sub>2</sub>O is through a hydrogen bond with the montmorillonite surface O, with the hydrogen bond distance of 195 pm. For the H<sub>2</sub>O molecular adsorption configuration, the adsorption energy is -2.6 eV. The H<sub>2</sub>O molecule bonds with the layer Ca<sup>2+</sup>, with the distance between the O atom of H<sub>2</sub>O and the layer Ca2+ atom being 226 pm. Additionally, H2O forms a hydrogen bond with the surface O atom, and the bond length of this hydrogen bond is 182 pm. This indicates that H<sub>2</sub>O can form a strong hydrogen bond with the montmorillonite surface. This strong hydrogen bond can further promote the dissociation of H<sub>2</sub>O. As shown in the H<sub>2</sub>O dissociative adsorption structure in Figure 7, the adsorption energy is -3.1 eV. The dissociated OH group bonds with layer Ca<sup>2+</sup>, with the Ca-O distance being 194 pm. The dissociated H atom bonds with a surface O atom, and the O-H bond length is 98 pm.





As can be seen from the above,  $\rm H_2O$  molecules are more likely to exist in a dissociated form on the surface of montmorillonite compared to molecular adsorption. Whether it is the dissociated adsorption of intact  $\rm H_2O$  molecules or the adsorption of a single OH group, they all adsorb onto the layer  $\rm Ca^{2+}$  and tend to form hydrogen bonds with the surface. The formation of hydrogen bonds in all these cases further stabilizes the adsorbed species. Understanding these surface-water interaction mechanisms is of great importance for comprehending related chemical processes, such as ion exchange reactions occurring on the montmorillonite surface.

# 3.3.2 $Ca^{2+}$ , $Na^+$ , $CO_3^{2-}$ and $SiO_3^{2-}$ absorbed montmorillonite

Figures 9, 10 display the structures and adsorption energies for the adsorption of  $\rm H_2O$  on  $\rm Ca^{2+}$ ,  $\rm Na^+$ ,  $\rm CO_3^{2-}$ , and  $\rm SiO_3^{2-}$  absorbed montmorillonite. The adsorption energy of  $\rm Ca\text{-}H_2O$  is -1.7 eV, which is lower than that of  $\rm H_2O$  on pristine montmorillonite (-3.1 eV). In this structure, the  $\rm H_2O$  molecule bonds with the layer  $\rm Ca^{2+}$ , with the distance between the O atom of  $\rm H_2O$  and the  $\rm Ca^{2+}$  atom being 232 pm. For Na- $\rm H_2O$ , the adsorption energy is -2.5 eV, which is stronger than  $\rm Ca\text{-}H_2O$ 

but comparable to  $\rm H_2O$  on clean montmorillonite. The  $\rm H_2O$  molecule bonds with surface  $\rm Na^+$ , with the O-Na bond distance being 229 pm.

In the  $CO_3$ - $H_2O$  and  $SiO_3$ - $H_2O$  structures, their adsorption energies are -1.2 eV and -1.1 eV, respectively. The adsorbed  $H_2O$  molecules form bonds with  $Ca^{2+}$  through O, with Ca-O bond distances of 239 pm and 236 pm, respectively.

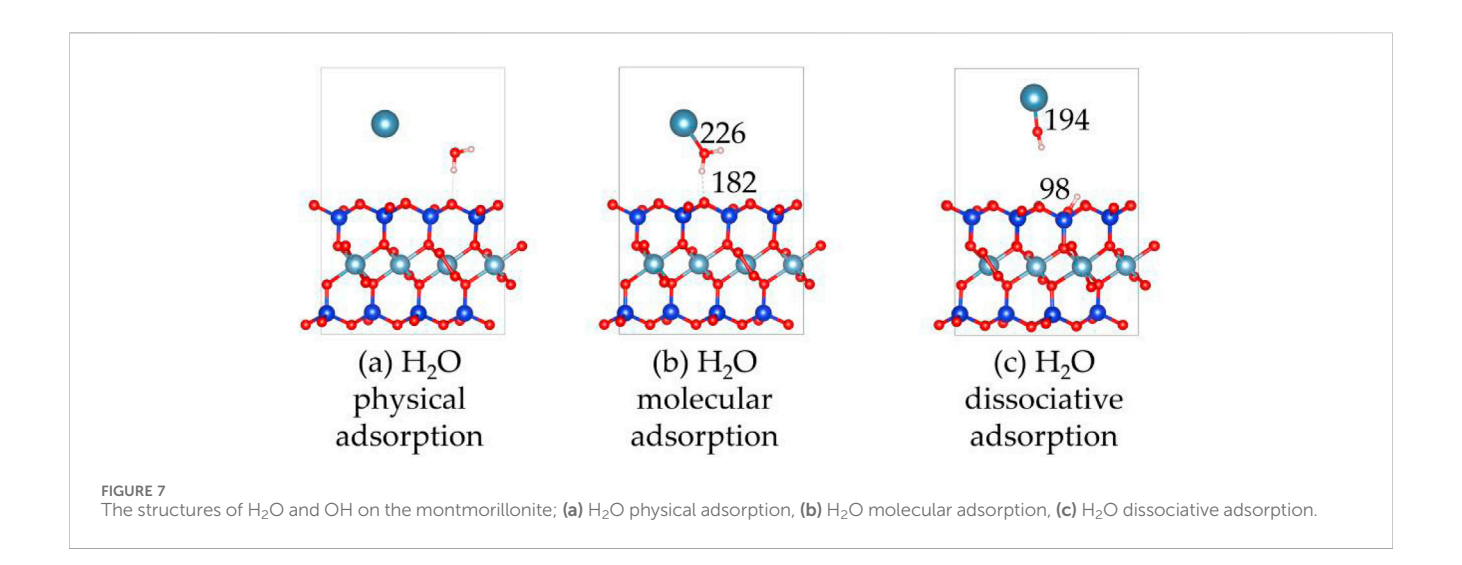
By comparing the adsorption of  $H_2O$  on pristine montmorillonite and montmorillonite adsorbed with  $Ca^{2+}$ ,  $Na^+$ ,  $CO_3^{2-}$ , and  $SiO_3^{2-}$ , it is evident that montmorillonite adsorbed with  $Ca^{2+}$ ,  $Na^+$ ,  $CO_3^{2-}$ , and  $SiO_3^{2-}$  inhibits water adsorption to different extents.

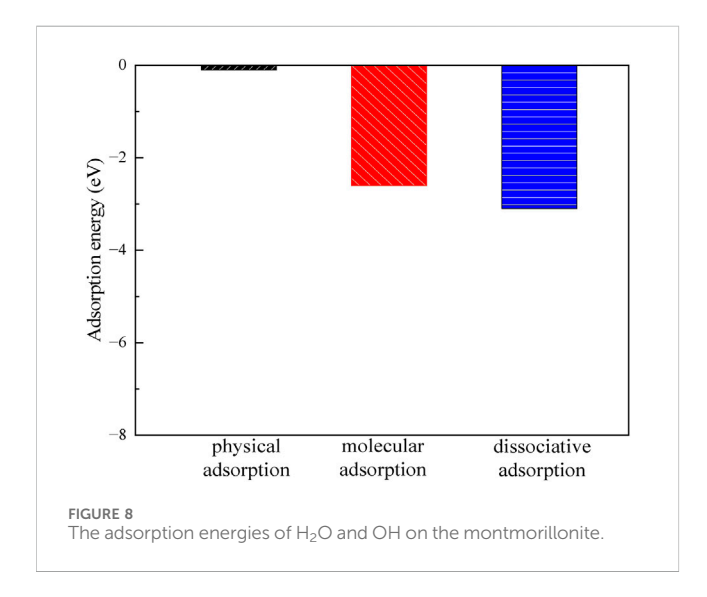
# 3.4 Adsorption mechanism from electronic structure

Figure 11 shows the differential charge density plots of  $Ca^{2+}$ ,  $Na^+$ ,  $CO_3^{2-}$  and  $SiO_3^{2-}$  on the on the montmorillonite surface.

It can be observed that there are significant changes in charge densities near the Ca2+ atoms and the surface O atoms of montmorillonite. Ca2+ atoms tend to lose electrons, characterized by a decrease in electron-cloud density (blue regions) around them. In contrast, the electron - cloud density around the surface O atoms that bond with Ca2+ increases (yellow regions). This indicates that during the adsorption of Ca<sup>2+</sup>, electrons are transferred from Ca2+ atoms to the surface atoms, forming ionic or polar covalent bonds. Such charge transfer  $Ca^{2+}$ enhances the interaction between and the montmorillonite surface. During the adsorption of Na+, the charge transfer is less intense compared to that of Ca<sup>2+</sup>. Therefore, in the figure, charge accumulation is only shown between the Na-O bonds.

When  $CO_3^{2^-}$  is adsorbed on the surface, there are notable changes in charge densities in the bonding regions between  $CO_3^{2^-}$  and the  $Ca^{2+}$  and Si atoms on the montmorillonite surface. There is an overlap and redistribution of electron clouds between the O atoms in  $CO_3^{2^-}$  and the  $Ca^{2+}$  and Si atoms. The increase in electron-cloud density around the O atoms indicates the inflow of electrons, leading to the formation of chemical bonds.





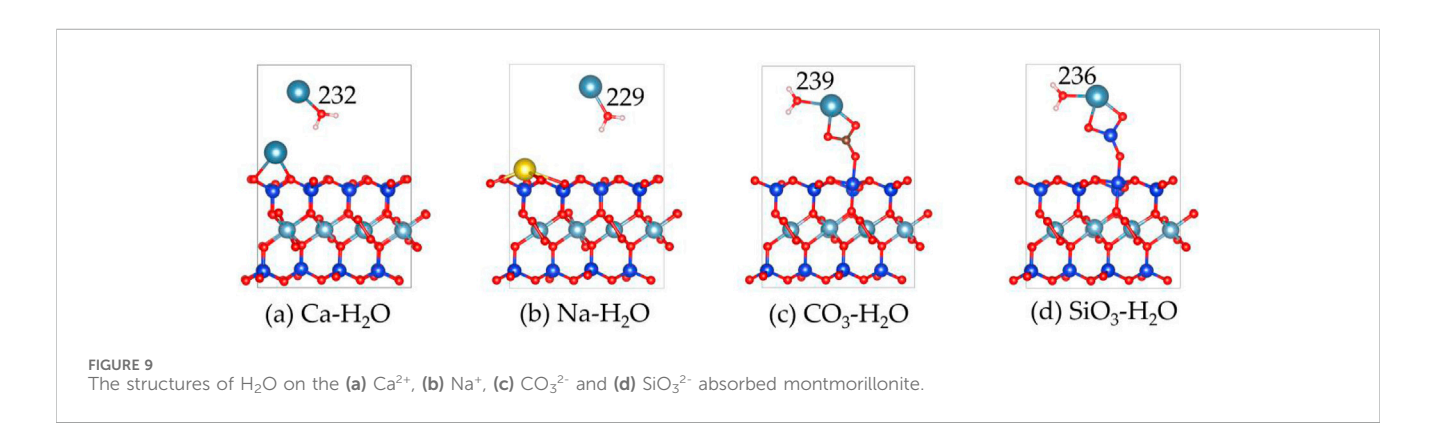
When  ${\rm SiO_3}^{2^-}$  is adsorbed on the surface, significant changes in electron-cloud densities occur at the bonding sites between the O atoms of  ${\rm SiO_3}^{2^-}$  and the  ${\rm Ca^{2^+}}$  and Si atoms on the montmorillonite surface. The electron-cloud enrichment around the O atoms (yellow regions) indicates that electrons

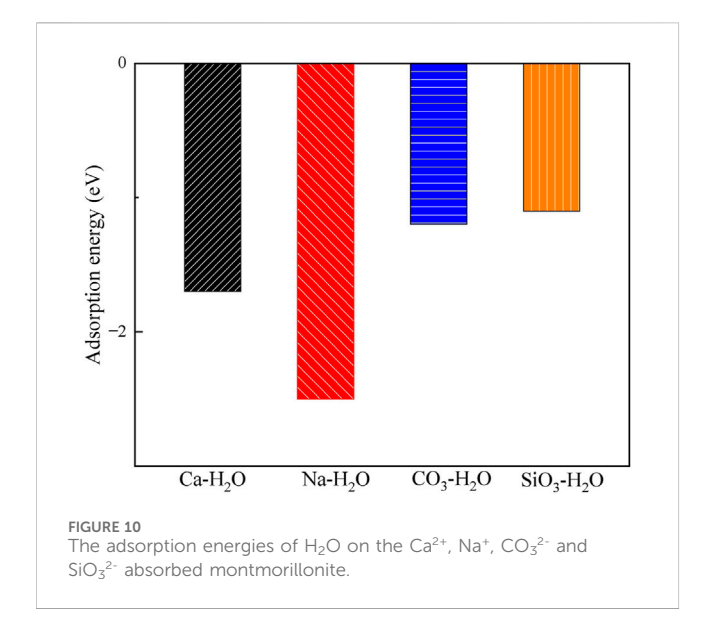
are transferred from the surface atoms to the O atoms, forming stable chemical bonds.

Table 3 shows the charge transfer between  $Ca^{2+}$ ,  $Na^+$ ,  $CO_3^{2-}$  and  $SiO_3^{2-}$  with the montmorillonite surface.  $Ca^{2+}$  and  $Na^+$  exhibit significantly stronger charge transfer with surface atoms than with interlayer Ca. Notably, the charge transfer between  $Na^+$  and interlayer  $Ca^{2+}$  is extremely weak, with a magnitude of only 0.03|e|. The charge transfer trends highlight that  $Ca^{2+}$  and  $Na^+$  primarily interact with montmorillonite surfaces through cationic charge donation, with  $Ca^{2+}$  exhibiting stronger binding due to higher charge transfer. In contrast, both  $CO_3^{2-}$  and  $SiO_3^{2-}$  demonstrate substantial charge transfer with both surface and interlayer  $Ca^{2+}$  atoms.  $CO_3^{2-}$  and  $SiO_3^{2-}$  form stable associations with both surface and interlayer  $Ca^{2+}$  via electron acceptance, consistent with the structural insights from differential charge density plots.

### 3.5 Comparison with alkaline OH treatment

The alkaline treatment process of montmorillonite has also been examined as shown in Figures 12, 13. The OH group adsorbs onto the Ca<sup>2+</sup> atom in the layer, forming a Ca-O bond with a bond length of 194 pm. Additionally, the OH group forms a hydrogen bond with





the surface, with a bond length of 251 pm, indicating the formation of a moderately strong hydrogen bond. The adsorption energy of the OH group is -6.5 eV, which is close to the -6.8 eV of  $CO_3^{2-}$ , but weaker than the -8.7 eV of  $SiO_3^{2-}$ .

Upon comparing the adsorption behaviors of hydroxide ions, carbonate ions, and silicate ions on the montmorillonite surface, it is observed that hydroxide ions primarily adsorb by forming hydrogen bonds with the surface, while carbonate and silicate ions adsorb via oxygensilicon bonds. Since the bond energy and stability of hydrogen bonds are weaker than those of oxygen-silicon bonds, this is one of the reasons why the strength of lime-treated soils is often lower than that of soils stabilized with lime combined with sodium silicate or sodium carbonate.

Furthermore, the hydrophilicity of OH-absorbed montmorillonite was calculated, revealing that its  $\rm H_2O$  adsorption energy is -1.3 eV. This value is weaker than the -2.6 eV of molecular adsorption (Figure 7b) and the -3.1 eV of dissociative adsorption (Figure 7c), indicating that after the absorption of OH, the water affinity of montmorillonite decreases.

The formation of a moderately strong hydrogen bond and the reduction in water affinity help explain why lime treatment can enhance the strength and water stability of soils.

### 3.6 The effect of CO<sub>2</sub> on stabilization

The structures of  $CO_2$  on the Ca-montmorillonite and  $CaCO_3$ -montmorillonite surface are shown in Figure 14. The adsorption energy of  $CO_2$  on the Ca-montmorillonite surface is calculated to be -0.2 eV. When  $CaCO_3$  forms on the montmorillonite surface, the adsorption energy of  $CO_2$  increases to -0.5 eV. These theoretical calculations suggest that the adsorption of  $CO_2$  by Ca-montmorillonite is thermodynamically favorable and is further enhanced by the nucleation of surface  $CaCO_3$ . This is consistent with the findings of Song et al. (2024), who reported that increased carbonate content promotes  $CO_2$  storage.

In addition, Liu et al. (2025) reported that increased water content promotes CO<sub>2</sub> adsorption. Under CO<sub>2</sub>-rich water conditions in deep underground environments, carbonate minerals can dissolve and recrystallize (Song et al., 2024), potentially affecting the stability of stabilized montmorillonite. This study focuses on improving the stability of stabilized montmorillonite near the Earth's surface, where both pressure and temperature are relatively low. Although the adsorption energy for CO<sub>2</sub> increases after nucleation, in practical engineering applications, the stabilizer-soil mixture is typically compacted at optimum water content, and the reaction products fill the pore spaces, increasing hydrophobicity. This significantly reduces water permeability of the stabilized soils, making it difficult to establish a CO<sub>2</sub>-rich water environment, thereby minimizing the risk of compromising stability and integrity.

## 3.7 Stabilization and hydrophilicity mechanisms

The schematic diagram illustrating the mechanisms of nucleation, stabilization, and hydrophilicity is shown in Figure 15. When CO<sub>3</sub><sup>2-</sup> or SiO<sub>3</sub><sup>2-</sup> ions are present in the Camontmorillonite system, they preferentially nucleate and form precipitates on the surface of montmorillonite rather than adsorb

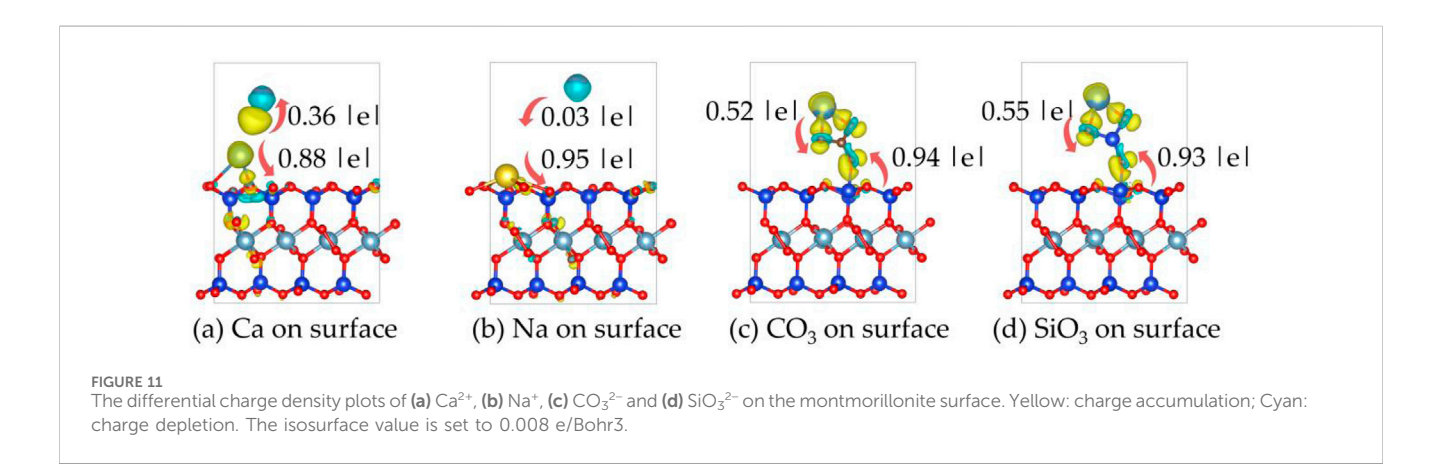
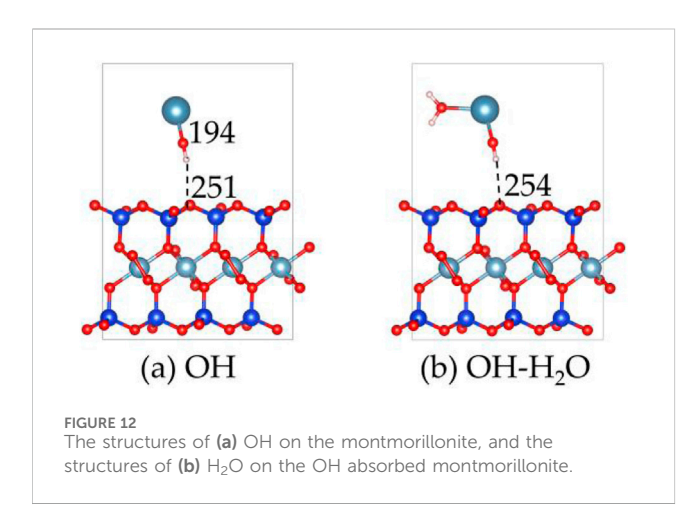
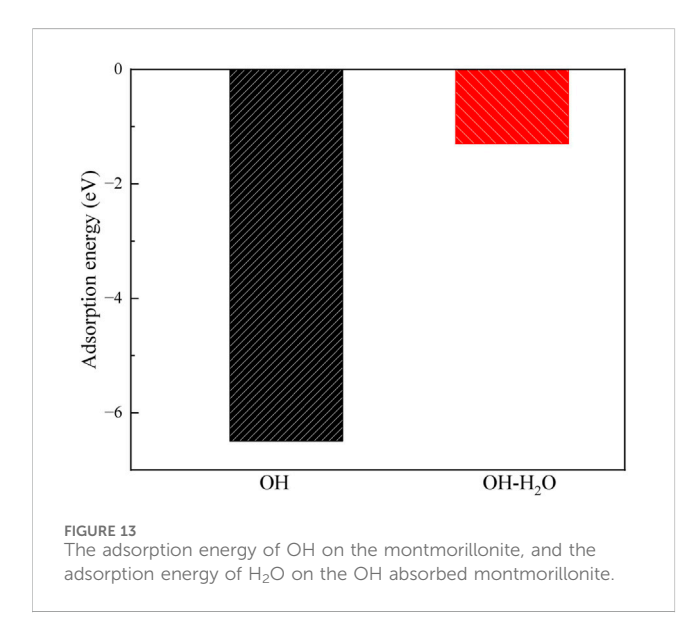


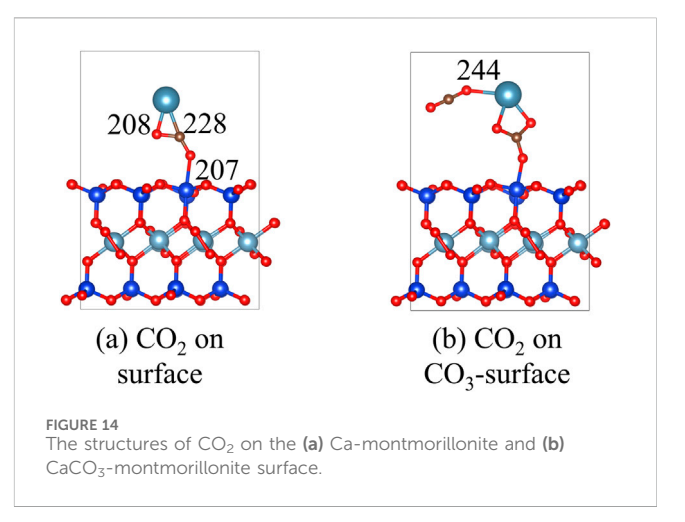
TABLE 3 Charge transfer between  ${\rm Ca^{2+}},\,{\rm Na^+},\,{\rm CO_3^{2-}}$  and  ${\rm SiO_3^{2-}}$  with the montmorillonite surface.

	Ca <sup>2+</sup>	Na <sup>+</sup>	CO <sub>3</sub> <sup>2-</sup>	SiO <sub>3</sub> <sup>2-</sup>	
Charge	1.24	0.92	-1.46	-1.48	





onto the interlayer calcium ions. This is because, compared to adsorption on interlayer calcium ions (Figures 3c,d), the adsorption energy is lower when the calcium ions are adsorbed and nucleation occurs on the montmorillonite surface (Figures 5c,d). The lower the adsorption energy, the more stable the system becomes. Therefore, it can be speculated that, when free calcium ions,  $CO_3^{2-}$  ions, and  $SiO_3^{2-}$  ions coexist in the calciumbased stabilized soil system, these ions tend to form a spatial network structure of calcium carbonate and calcium silicate on the

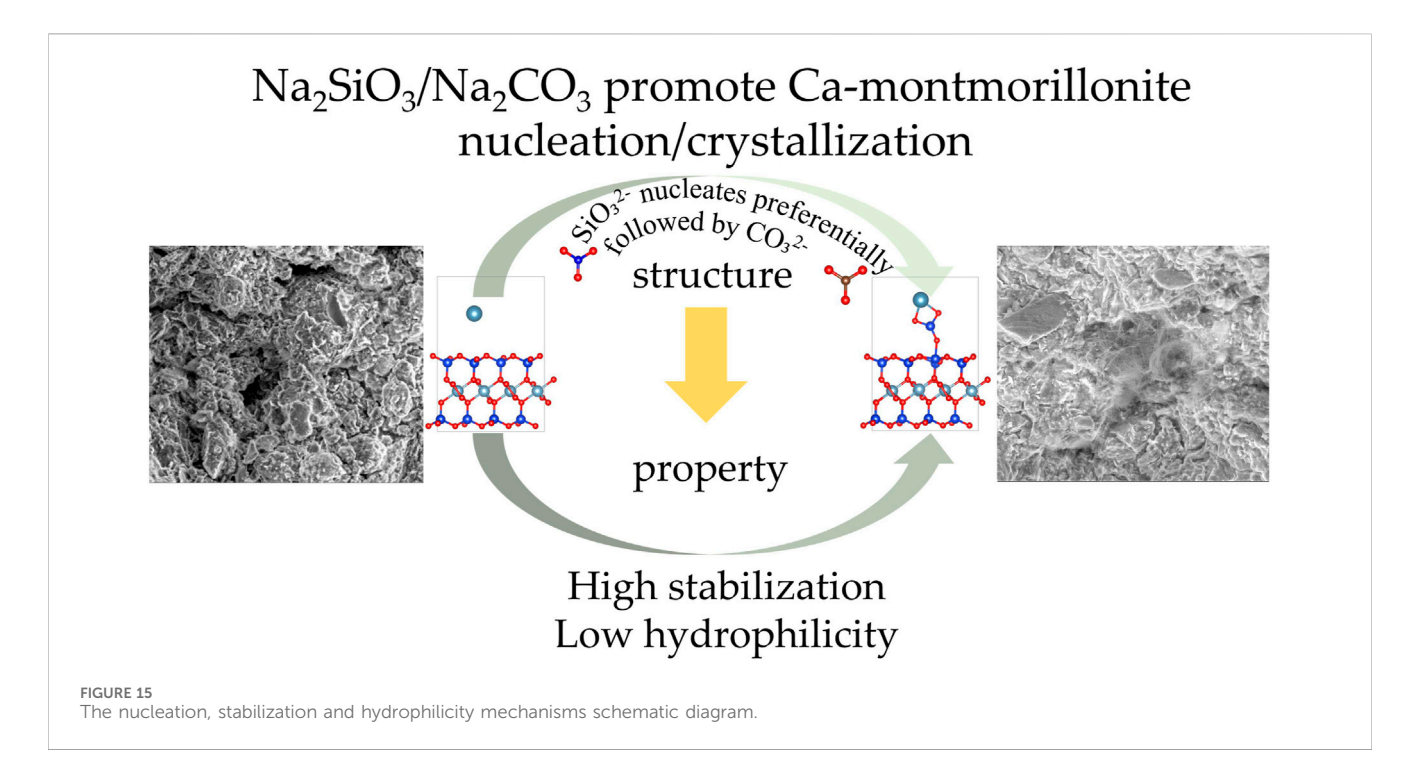


montmorillonite surface and within the pores through the sharing of calcium ions. This process enhances the overall integrity of montmorillonite, thereby improving its shear strength. This hypothesis aligns with the results observed in the SEM images (Figure 2).

Before stabilization, except for physical absorption (Figure 7a), the adsorption energies of water molecules in the interlayers of montmorillonite are relatively negative, and they are prone to adsorb through molecular absroption (Figure 7b) and dissociative adsorption (Figure 7c). This explains the strong hydrophilicity of montmorillonite, volume expansion after water absorption, and reduced macroscopic engineering properties. After stabilization, Na<sup>+</sup> has almost minor effect on the hydrophilicity of montmorillonite, while Ca<sup>2+</sup>, CO<sub>3</sub><sup>2-</sup> or SiO<sub>3</sub><sup>2-</sup> significantly reduce its hydrophilicity. This can explain that calcium-based stabilizer alone, or in combination with Na<sub>2</sub>CO<sub>3</sub> and Na<sub>2</sub>SiO<sub>3</sub> can ruduce the affinity of montmorillonite for water.

By comparing the water adsorption energy of Camontmorillonite (Figure 5a) and Na-montmorillonite (Figure 5b), the calcium ions released by calcium-based stabilizer will exchange with Na<sup>+</sup> and other ions through ion exchange, thus reducing the thickness of the water film. However, by comparing the reduction in water adsorption energy between montmorillonite adsorbed with calcium ions (Figure 9a) and montmorillonite adsorbed with calcium carbonate (Figure 9c) and calcium silicate (Figure 9d), it is evident that the improvement in water stability due to ion exchange is weaker than the improvement by the formation of precipitates.

The results above demonstrate that DFT calculations can effectively and quantitatively elucidate the interaction mechanisms between stabilizers and montmorillonite from the perspective of adsorption energy and electron transfer. This method can transform the selection of stabilizer components from a trial-and-error approach into a more targeted process based on the understanding of the interactions between clay minerals and candidates, reducing time-consuming, labor-intensive macro-mechanical tests and saving experimental costs. The DFT method is expected to not only enhance material screening



for soil stabilization but also have broader applications in areas such as carbon sequestration, landfills, and beyond.

### 4 Conclusion

In this work, experiments and DFT calculation were used to investigate the stabilization and hydrophilicity mechanisms of Camontmorillonite systems modified with  $Na_2CO_3$  and  $Na_2SiO_3$ .

- 1.  $SiO_3^{2-}$  and  $CO_3^{2-}$  ions preferentially adsorb on the montmorillonite surface rather than the exchangeable interlayer, with significantly higher adsorption energies compared to  $Ca^{2+}$  and  $Na^+$  ions.
- The nucleation mechanism involves the bonding of O atoms from SiO<sub>3</sub><sup>2-</sup> and CO<sub>3</sub><sup>2-</sup> ions to the montmorillonite surface Si and Ca<sup>2+</sup> ions in the interlayer, leading to the formation of CaSiO<sub>3</sub> and CaCO<sub>3</sub> network structures.
- 3. Adsorption of  $Ca^{2+}$ ,  $Na^+$ ,  $CO_3^{2-}$ , and  $SiO_3^{2-}$  ions on the montmorillonite reduces the adsorption of  $H_2O$ , lowering the water adsorption energy from -3.1 eV to -1.1 to -2.5 eV.
- 4. Na<sub>2</sub>CO<sub>3</sub> and Na<sub>2</sub>SiO<sub>3</sub> enhance the nucleation of CaSiO<sub>3</sub> and CaCO<sub>3</sub> on the montmorillonite surface, improving interfacial interactions and reducing water affinity. This has potential applications in reducing caprock permeability in saline aquifers for CO<sub>2</sub> storage and improving the compressive strength and water resistance of stabilized soils in soil stabilization.

### Data availability statement

The original contributions presented in the study are included in the article/supplementary material, further inquiries can be directed to the corresponding author.

### **Author contributions**

CY: Conceptualization, Writing – review and editing, Methodology, Formal Analysis, Software, Writing – original draft. JH: Writing – original draft, Methodology, Formal Analysis, Software, Conceptualization. S-YD: Formal Analysis, Software, Writing – original draft. CM: Writing – original draft, Writing – review and editing, Methodology, Formal Analysis. YP: Conceptualization, Methodology, Writing – original draft, Formal Analysis, Writing – review and editing.

### **Funding**

The author(s) declare that financial support was received for the research and/or publication of this article. This research was funded by Zhejiang Shuren University Research Project, grant number 2023R026.

### **Acknowledgments**

This is a short text to acknowledge the contributions of specific colleagues, institutions, or agencies that aided the efforts of the authors.

### Conflict of interest

The authors declare that the research was conducted in the absence of any commercial or financial relationships that could be construed as a potential conflict of interest.

### Generative AI statement

The author(s) declare that no Generative AI was used in the creation of this manuscript.

Any alternative text (alt text) provided alongside figures in this article has been generated by Frontiers with the support of artificial intelligence and reasonable efforts have been made to ensure accuracy, including review by the authors wherever possible. If you identify any issues, please contact us.

### References

Abdullah, H. H., Shahin, M. A., Walske, M. L., and Karrech, A. (2021). Cyclic behaviour of clay stabilised with fly-ash based geopolymer incorporating ground granulated slag. *Transp. Geotech.* 26, 100430. doi:10.1016/j.trgeo.2020.100430

Anburuvel, A. (2023). The engineering behind soil stabilization with additives: a state-of-the-art review.  $Geotechnical\ Geol.\ Eng.\ 42,\ 1-42.\ doi:10.1007/s10706-023-02554-x$ 

Barman, D., and Dash, S. K. (2022). Stabilization of expansive soils using chemical additives: a review. *J. Rock Mech. Geotechnical Eng.* 14, 1319–1342. doi:10.1016/j.jrmge. 2022.02.011

Bell, F. G. (1996). Lime stabilization of clay minerals and soils. *Eng. Geol.* 42, 223–237. doi:10.1016/0013-7952(96)00028-2

Blöchl, P. E. (1994). Projector augmented-wave method. Phys. Rev. B 50, 17953–17979. doi:10.1103/physrevb.50.17953

Cao, J., Liu, F., Huang, S., Kong, C., Sun, H., Gao, Y., et al. (2022). Influence of humic acid on the strength of cement-soil and analysis of its microscopic mechanism. *Adv. Civ. Eng.* 2022, 1554204. doi:10.1155/2022/1554204

Chatterjee, A., Iwasaki, T., Ebina, T., and Miyamoto, A. (1999). A DFT study on clay-cation-water interaction in montmorillonite and beidellite. *Comput. Mater. Sci.* 14, 119–124. doi:10.1016/s0927-0256(98)00083-4

Chung, H., Kim, S. H., and Nam, K. (2021). Application of microbially induced calcite precipitation to prevent soil loss by rainfall: effect of particle size and organic matter content. *J. Soils Sediments* 21, 2744–2754. doi:10.1007/s11368-020-02757-2

Dengliang, Z. Y. X., and Aimin, S. (1988). Experimental study on early strength of lime-fly ash stabilized soil. *J. Chang. Univ. Nat. Sci. Ed.*, 12–24.

Fonseca, C. G., Vaiss, V. S., Wypych, F., Diniz, R., and Leitão, A. A. (2018). Investigation of the initial stages of the montmorillonite acid-activation process using DFT calculations. *Appl. Clay Sci.* 165, 170–178. doi:10.1016/j.clay.2018.08.012

França, D., Oliveira, L., Nunes Filho, F., Silva Filho, E., Osajima, J., Jaber, M., et al. (2022). The versatility of montmorillonite in water remediation using adsorption: current studies and challenges in drug removal. *J. Environ. Chem. Eng.* 10, 107341. doi:10.1016/j.jece.2022.107341

Giese, R. F., and Van Oss, C. J. (2002). Colloid and surface properties of clays and related minerals. Boca Raton, Florida: CRC Press, Vol. 105.

Guo, F., Li, D., Fein, J. B., Xu, J., Wang, Y., Huang, Q., et al. (2022). Roles of hydrogen bond and ion bridge in adsorption of two bisphenols onto montmorillonite: an experimental and DFT study. *Appl. Clay Sci.* 217, 106406. doi:10.1016/j.clay.2022.106406

Huang, W. J., Liu, J. H., She, Q. M., Zhang, J. Q., and Zhou, C. H. (2023). Recent advances in engineering montmorillonite into catalysts and related catalysis. *Catal. Rev.* 65, 929–985. doi:10.1080/01614940.2021.1995163

Jiang, N., Wang, C., Wang, Z., Li, B., and Liu, Y.-a. (2021). Strength characteristics and microstructure of cement stabilized soft soil admixed with silica fume. *Materials* 14, 1929. doi:10.3390/ma14081929

Kühne, T. D., Iannuzzi, M., Del Ben, M., Rybkin, V. V., Seewald, P., Stein, F., et al. (2020). CP2K: an electronic structure and molecular dynamics software package quickstep: efficient and accurate electronic structure calculations. *J. Chem. Phys.* 152, 194103. doi:10.1063/5.0007045

Li, T., Chai, Z., Yang, Z., Xin, Z., Sun, H., and Yan, K. (2023). Insights into the influence mechanism of different interlayer cations on the hydration activity of montmorillonite surface: a DFT calculation. *Appl. Clay Sci.* 239, 106965. doi:10. 1016/j.clay.2023.106965

Liu, Y., Ren, J., Bhawangirkar, D. R., Zhao, J., Linga, P., and Yin, Z. (2025). Thermodynamic inhibition of CO2 hydrate by Na-montmorillonite: implications for hydrate-based CO2 sequestration. *Carbon Neutrality* 4, 18. doi:10.1007/s43979-025-00132-z

Ma, C., Chen, B., and Chen, L. (2018). Experimental feasibility research on a high-efficiency cement-based clay stabilizer. *KSCE J. Civ. Eng.* 22, 62–72. doi:10.1007/s12205-017-0782-8

### Publisher's note

All claims expressed in this article are solely those of the authors and do not necessarily represent those of their affiliated organizations, or those of the publisher, the editors and the reviewers. Any product that may be evaluated in this article, or claim that may be made by its manufacturer, is not guaranteed or endorsed by the publisher.

Mitchell, J. K., and Soga, K. (2005). Fundamentals of soil behavior. New York: John Wiley and Sons. Vol. 3.

Murmu, A. L., Dhole, N., and Patel, A. (2020). Stabilisation of Black cotton soil for subgrade application using fly ash geopolymer. *Road Mater. Pavement Des.* 21, 867–885. doi:10.1080/14680629.2018.1530131

Peng, C., Min, F., Liu, L., and Chen, J. (2016). A periodic DFT study of adsorption of water on sodium-montmorillonite (001) basal and (010) edge surface. *Appl. Surf. Sci.* 387, 308–316. doi:10.1016/j.apsusc.2016.06.079

Petry, T. M., and Little, D. N. (2002). Review of stabilization of clays and expansive soils in pavements and lightly loaded structures—history, practice, and future. *J. Mater. Civ. Eng.* 14, 447–460. doi:10.1061/(ASCE)0899-1561(2002)14:6(447)

Phummiphan, I., Horpibulsuk, S., Sukmak, P., Chinkulkijniwat, A., Arulrajah, A., and Shen, S.-L. (2016). Stabilisation of marginal lateritic soil using high calcium fly ashbased geopolymer. *Road Mater. Pavement Des.* 17, 877–891. doi:10.1080/14680629. 2015.1132632

Puppala, A. J. (2016). Advances in ground modification with chemical additives: from theory to practice. *Transp. Geotech.* 9, 123–138. doi:10.1016/j.trgeo.2016.08.004

Raja, P. S. K., and Thyagaraj, T. (2020). Sulfate effects on sulfate-resistant cement–treated expansive soil. *Bull. Eng. Geol. Environ.* 79, 2367–2380. doi:10.1007/s10064-019-01714-9

Rivera, J. F., Orobio, A., Cristelo, N., and de Gutierrez, R. M. (2020). Fly ash-based geopolymer as A4 type soil stabiliser. *Transp. Geotech.* 25, 100409. doi:10.1016/j.trgeo.

Song, Z., Yang, L., Jiang, F., Zhu, W., Li, X., Qi, Z., et al. (2024). The mechanism of clay mineral transformation in CO2 geological storage and its impact on long-term storage potential. *Geoenergy Sci. Eng.* 242, 213192. doi:10.1016/j.geoen.2024.213192

Teerawattanasuk, C., and Voottipruex, P. (2019). Comparison between cement and fly ash geopolymer for stabilized marginal lateritic soil as road material. *Int. J. Pavement Eng.* 20, 1264–1274. doi:10.1080/10298436.2017.1402593

VandeVondele, J., and Hutter, J. (2007). Gaussian basis sets for accurate calculations on molecular systems in gas and condensed phases. *J. Chem. Phys.* 127, 114105. doi:10. 1063/1.2770708

Wang, Y., Liu, Z., Wan, W., Nie, A., Zhang, Y., and Han, C. (2023). Toughening effect and mechanism of rice straw fiber-reinforced lime soil. *Constr. Build. Mater.* 393, 132133. doi:10.1016/j.conbuildmat.2023.132133

Wu, J., Feng, M., Mao, X., Xu, J., Zhang, W., Ni, X., et al. (2018). Particle size distribution of aggregate effects on mechanical and structural properties of cemented rockfill: experiments and modeling. *Constr. Build. Mater.* 193, 295–311. doi:10.1016/j. conbuildmat.2018.10.208

Yin, C., Zhang, W., Jiang, X., and Huang, Z. (2018). Effects of initial water content on microstructure and mechanical properties of lean clay soil stabilized by compound calcium-based stabilizer. *Materials* 11, 1933. doi:10.3390/ma11101933

Yin, C., Deng, S., Zhao, J., Tao, Y., and Huang, J. (2025). Effects of non-traditional additives on the early strength of a lean clay soil stabilized by compound calcium-based stabilizer. *Period. Polytech. Civ. Eng.* 69, 752–762. doi:10.3311/ppci.37150

Yu, H., Joshi, P., Lau, C., and Ng, K. (2024). Novel application of sustainable coal-derived char in cement soil stabilization. *Constr. Build. Mater.* 414, 134960. doi:10.1016/j.conbuildmat.2024.134960

Zada, U., Jamal, A., Iqbal, M., Eldin, S. M., Almoshaogeh, M., Bekkouche, S. R., et al. (2023). Recent advances in expansive soil stabilization using admixtures: current challenges and opportunities. *Case Stud. Constr. Mater.* 18, e01985. doi:10.1016/j.cscm.2023.e01985

Zhu, R., Chen, Q., Zhou, Q., Xi, Y., Zhu, J., and He, H. (2016). Adsorbents based on montmorillonite for contaminant removal from water: a review. *Appl. Clay Sci.* 123, 239–258. doi:10.1016/j.clay.2015.12.024